

Article

Effect of Al Substitution on Structural, Magnetic, and Magnetocaloric Properties of $\text{Er}_6\text{Fe}_{23-x}\text{Al}_x$ ($x = 0$ and 3) Intermetallic Compounds

M. Jemmali ^{1,2,*}, S. Alleg ³, E. Dhahri ⁴ and L. Bessais ⁵

¹ Laboratoire des Sciences des Matériaux et de l'Environnement,

Faculté des Sciences de Sfax-Université de Sfax, BP 1171, 3018 Sfax, Tunisie

² Chemistry Department, College of Science and Arts at Ar-Rass, Qassim University,

P.O. Box53, Buraydah 51452, Saudi Arabia

³ Laboratoire de Magnétisme et Spectroscopie des Solides, Département de Physique, Faculté des Sciences,

Université Badji Mokhtar-Annaba, B.P. 12, Annaba 23000, Algeria; safia_alleg@yahoo.fr

⁴ Laboratoire de Physique appliqué, Département de Physique, Faculté des Sciences de Sfax, 3018 Sfax,

Tunisie; essebti@yahoo.com

⁵ Université Paris Est, ICMPE (UMR 7182), CNRS, UPEC, THIAIS F-94320, France; bessais@icmpe.cnrs.fr

* Correspondence: jmosbah73@gmail.com

Academic Editor: Alex V. Morozkin

Received: 16 April 2017; Accepted: 13 May 2017; Published: 27 May 2017

Abstract: The structural, magnetic, and magnetocaloric properties of $\text{Er}_6\text{Fe}_{23-x}\text{Al}_x$ ($x = 0$ and 3) intermetallic compounds have been studied systematically. Samples were prepared using the arc furnace by annealing at 1073 K for one week. Rietveld analysis of XRD shows the formation of pure crystalline phase with cubic Fm-3m structure. Refinement results show that the unit cell volume decreases with increasing Al content. The Curie temperature T_c of the prepared samples was found to be strongly dependent on the aluminum content. This reduces magnetization and the ferrimagnetic phase transition temperature (T_c) from 481 K (for $x = 0$) to 380 K (for $x = 3$), is due to the substitution of magnetic element (Fe) by non-magnetic atoms (Al). With the increase of the Al content, a decrease in the values of magnetic entropy is observed. The magnitude of the isothermal magnetic entropy ($|\Delta SM|$) at the T_c decreases from 1.8 J/kg·K for $x = 0$ to 0.58 J/kg·K for $x = 3$ for a field change 14 kOe. Respectively, the relative cooling power (RCP) decreases with increasing Al content reaching 42 Jkg⁻¹ for $x = 0$ to 28 Jkg⁻¹ for $x = 3$.

Keywords: intermetallic; rare earth; crystal structure; magnetocaloric effect; relative cooling power

1. Introduction

Intermetallic compounds that contain rare-earth elements are particularly interesting because of their temperature- and pressure-dependent structural and physical transitions that make them potential candidates for magnetic applications [1–9].

Investigations on the structure and the magnetic properties of R_6M_{23} ($\text{M} = \text{Mn}, \text{Fe}$) have been reported in the literature [10]. It was found that R_6Fe_{23} compounds crystallize in $\text{Th}_6\text{Mn}_{23}$ type structure and with a space group of Fm-3m.

Rare earth 4f-Transition metals 3d intermetallic compounds of 6:23 stoichiometry show very interesting magnetic properties [11]. The magnetic characterization of the rare earth 5d states is of special significance for the magnetic properties of the R–M materials as they mediate the magnetic interaction between the R and M sublattices [12].

$\text{Er}_6\text{Fe}_{23}$ is of great interest among the compounds in the Er–Fe system, because it contains a large amount of iron in the unit cell. There are 116 atoms per unit cell occupying five non-equivalent crystal

sites (24e, 4b, 24d, 32f₁, and 32f₂). The magnetic properties of Er₆Fe₂₃ were studied by Boltich et al. [10]. This compound presents compensation temperature at 95 K and a ferrimagnetic behavior at 493 K. However, there have been few studies on Er₆Fe₂₃ since then. This seems to be due to the difficulty entailed in preparing the Er₆Fe₂₃ intermetallic compound.

Neutronic study on Dy₆Mn₂₃ and Er₆Mn₂₃ [13] shows that this collinear ferromagnetic arrangement of the Mn sublattice persists at low temperature when the R sublattice is ordered. Both neutron diffraction study and magnetization measurements on single crystals [13–15] provide that the R sublattice then adopts a complex non-collinear magnetic order. More importantly, the R–Mn exchange coupling is stronger with the 24d and 4b sites than with the 32f₁ and 32f₂ sites. This yields a behavior in apparent contradiction with the usual sign of the R–Mn coupling in intermetallic: in R₆Mn₂₃ the low temperature magnetization is higher with the heavy lanthanides than with the light ones [16–19].

In the present work, we focused on the preparation, structure, magnetic properties, and magnetocaloric of the Er₆Fe_{23–x}Al_x (x = 0 and 3) compounds and the influence of Al on the magnetic properties.

2. Experimental

Polycrystalline samples of Er₆Fe_{23–x}Al_x (x = 0 and 3) were synthesized by arc-melting stoichiometric amounts of the constituent elements: Fe, Er, and Al (with purity 99.99%) under protective argon atmosphere. The pellets were turned over and remelted several times, in order to ensure a good homogeneity. The samples were wrapped in a tantalum sheet and annealed at 1073 K for one week to improve the atomic diffusion kinetics and to ensure a good crystallinity. After arc-melting, these alloys were finished by direct water quenching of the pellets from the furnace. The intermetallics were ground to powder by means of a mortar to prepare them for measurements. The powders were sieved using a 40 μm pore size metallic sieve.

The final product was characterized using powder X-ray diffraction (XRD) on a Brucker diffractometer (Brucker, Thiais, France) using copper radiation ($\lambda K\alpha_1 = 1.540600 \text{ \AA}$, $\lambda K\alpha_2 = 1.544390 \text{ \AA}$) to determine the crystallographic structure and identify the present phase. Forty milligrams of powder was loaded on a sample holder as a randomly oriented powder. Scans of 2θ between 20° and 80° with steps 0.015° and counting times of 13.5 s per point were measured at 300 K. In this latter procedure, the Bragg peak breadth is a combination of both instrument and sample dependent effects. To remove these aberrations, it is necessary to assemble a diffraction pattern from the line broadening of a standard material with a good crystallinity such as silicon, to determine the instrumental broadening. Silicon is added as an internal standard, the pattern is established by the Rietveld process [20] using Fullprof code as a single-phase pattern. The Si unit-cell parameter fixed at $a = 12.4312 \text{ \AA}$ and $U = 0.007754$, $V = -0.010764$, and $W = 0.005756$. The data of Er₆Fe₂₀Al₃ were analyzed and refined with the same technique of refinement using for silicon. U, V, W-half-width parameters normally characterize the instrumental resolution function.

The magnetic and magnetocaloric measurements of the sample were performed using the Physical Properties Measurement System PPMS9 (Quantum Design), at low temperature, under an applied field up to 5 T in a temperature range from 10 K to 300 K and by the magnetometer SQUID: (Superconducting QUantum Interference Device) at high temperature, between 300 K and 500 K (for magnetic and magnetocaloric measurement).

3. Results and Discussion

3.1. X-ray Diffraction Results

Erbium ternary compounds of the Er–Fe–Al system contain a large number of intermetallic compounds were constructed at 1073 K in our laboratory [21]. We extended our investigation in a systematic search of new interesting intermetallic compounds in this ternary diagram, and confirmed a

significant extension by the X-ray analysis. This result showed that the samples contained single phase of $\text{Er}_6\text{Fe}_{23-x}\text{Al}_x$ ($x = 0$ and 3). A comparison of the X-ray diffraction patterns of the $\text{Er}_6\text{Fe}_{23-x}\text{Al}_x$ ($x = 0$ and 3) compounds revealed that there is no change in the patterns, except the shift in position of Bragg reflections, towards higher angle sides, indicating variation in the lattice parameters. The index results of X-ray diffraction patterns indicated that all the alloys crystallizes in the cubic $\text{Th}_6\text{Mn}_{23}$ -type crystal structure, $\text{Th}_6\text{Mn}_{23}$ -type structure with space group Fm-3m and lattice parameters $a = 11.991\text{--}12.068 \text{ \AA}$. The variation of the unit cell parameters shows that the unit-cell parameters decrease with the increase of Al contents. There are 116 atoms per unit cell occupying five non equivalent crystal sites (24e, 4a, 24d, 32f₁, and 32f₂). The 24e positions are accessible only to the rare earth atoms, whereas iron atoms occupy the other positions.

The analysis of the XRD patterns of the $\text{Er}_6\text{Fe}_{20}\text{Al}_3$ compound shows that this system crystallizes in the cubic $\text{Th}_6\text{Mn}_{23}$ -type structure and Fm-3m space group. The lattice parameter is: $a = 12.0082(2) \text{ \AA}$. This value is slightly smaller than that of $\text{Er}_6\text{Fe}_{23}$ ($a = 12.01(3) \text{ \AA}$) [22]; in agreement with a simple steric effect of Al ($r_{\text{Fe}} = 1.26 \text{ \AA}$) substitution by a bigger atom ($r_{\text{Al}} = 1.43 \text{ \AA}$). The representative Rietveld refinement results for $\text{Er}_6\text{Fe}_{20}\text{Al}_3$ are shown in Figure 1 and listed in Table 1. The observed and the calculated diffraction patterns for $\text{Er}_6\text{Fe}_{20}\text{Al}_3$ at room temperature match well and show that the sample contains the single $\text{Th}_6\text{Mn}_{23}$ phase.

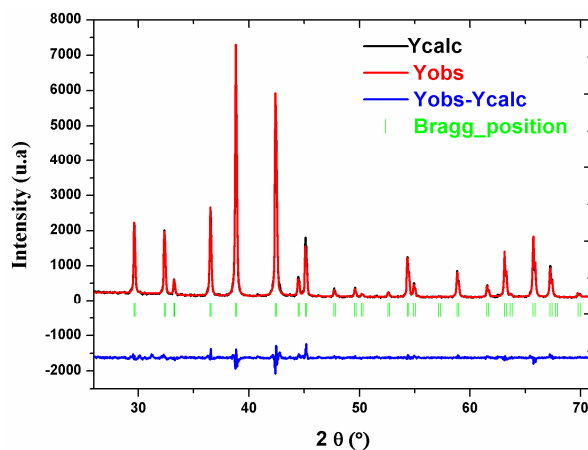


Figure 1. Rietveld refinement of $\text{Er}_6\text{Fe}_{20}\text{Al}_3$ compound.

Table 1. Details of structure refinement for $\text{Er}_6\text{Fe}_{20}\text{Al}_3$.

Compound	$\text{Er}_6\text{Fe}_{20}\text{Al}_3$
Type structure	$\text{Th}_6\text{Mn}_{23}$
Space group	Fm-3m
Cell parameters:	
A (\AA)	12.0082(2)
Volume (\AA^3)	1748.91(3)
D_{cal} ($\text{g}\cdot\text{cm}^{-3}$)	7.199
R_{Bragg}	3.21
R_{factor}	2.37
Rp	6.68
Rwp	8.58
$\chi^2 = \left[\frac{R_{\text{wp}}}{R_{\text{exp}}} \right]^2$ (%)	2.26

We have determined the distribution of Al atoms over the three possible Fe crystallographic sites. According to the Rietveld refinement and especially to the occupation refinement, we demonstrated and determined that the Al atoms are distributed in three crystallographic sites: 32f₁, 32f₂, and 24d. The best agreement factors R_{F} and R_{B} of the $\text{Er}_6\text{Fe}_{20}\text{Al}_3$ compound have been obtained with Al located

in the $32f_1$, $32f_2$, and $24d$ (Table 2). In fact, in our groups, we have proven in the $\text{Er}_6\text{Fe}_{17.66}\text{Al}_{5.34}\text{C}_{0.65}$ compound [23] that only one of the two $32f$ sites exhibited a significant deviation from the full occupancy with Fe atoms, indicating a substitution with Al atoms. Carbon atoms in this compound localized a new octahedral site. However, with the same structure type, Lemoine et al. [24] did not demonstrate the distribution of Co in the $\text{Gd}_6(\text{Mn}_{1-x}\text{Co}_x)_{23}$ system.

Table 2. Atomic coordinates, occupations, and equivalent isotropic displacement parameters for $\text{Er}_6\text{Fe}_{20}\text{Al}_3$.

Atoms	Sites	x	y	z	Occ	Ueq
Fe1	$32f_1$	0.1215(2)	0.1215(3)	0.1215(3)	0.890(2)	0.037(6)
Al1	$32f_1$	0.1215(2)	0.1215(3)	0.1215(3)	0.091(2)	0.037(6)
Fe2	$32f_2$	0.3234(2)	0.3234(2)	0.3234(2)	0.880(2)	0.021(6)
Al2	$32f_2$	0.3234(2)	0.3234(2)	0.3234(2)	0.110(2)	0.021(6)
Fe3	$24d$	0.00000	0.25000	0.25000	0.740(2)	0.023(6)
Al3	$24d$	0.00000	0.25000	0.25000	0.259(1)	0.023(6)
Fe4	$4a$	0.00000	0.00000	0.00000	1.00	0.011(5)
Er	$24e$	0.2978(2)	0.00000	0.00000	1.00	0.001(4)

$$U_{eq} (\text{\AA}^2) = 1/3 \sum_i \sum_j U_{ij} a_i^* a_j^* a_i a_j.$$

In the structure of $\text{Er}_6\text{Fe}_{20}\text{Al}_3$ Figure 2, all metal atoms have high coordination numbers, as is usually the case for intermetallic phases. The Er atoms are coordinated by 12 Fe/Al, one Fe, and four Er atoms. The Er–Er distances of 3.445(2) Å are rather large, considering the metallic radius of erbium for the coordination number (CN) 17. Nevertheless, if one discounts these erbium neighbors, the coordination polyhedron of the erbium atom would look rather incomplete. The Er–Fe/Al or Er–Fe distances cover the range between 2.963(3) Å and 3.588(2) Å.

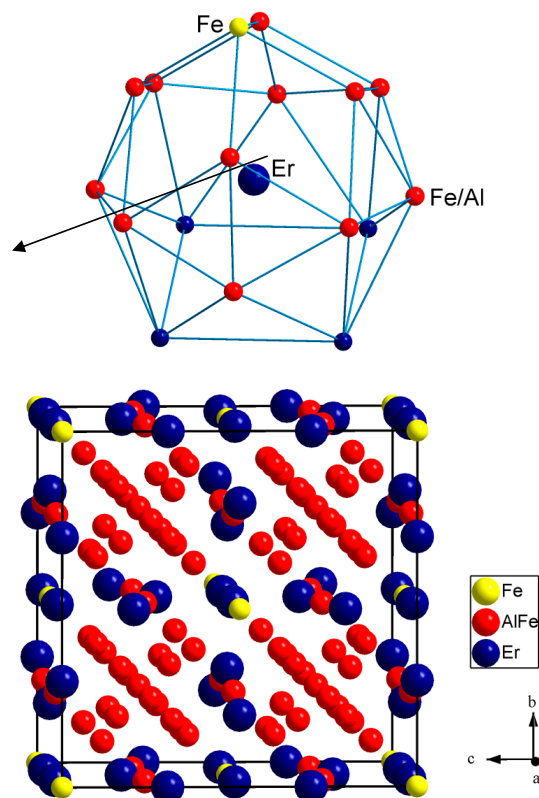


Figure 2. Crystal structure of $\text{Er}_6\text{Fe}_{20}\text{Al}_3$ compound and Er coordination.

3.2. Magnetic Properties

The Curie temperature is a direct measure of the exchange interaction, which is the origin of ferromagnetism. This interaction depends on the interatomic distance. In fact, T_C is determined by three kinds of exchange interactions: 3d–3d exchange interaction between magnetic Fe moment sublattice, 4f–4f exchange interaction between the magnetic moments of rare earth sublattice and the inter-sublattice 3d–4f and 3d–5d exchange interaction, which probably favor a ferrimagnetic collinear structure and the anisotropies of the Er, Al, and Fe sites had to be considered.

Figure 3 shows the thermomagnetic curve of $\text{Er}_6\text{Fe}_{23-x}\text{Al}_x$ with $x = 0$ and 3. The value of T_C (which are flagged with arrows) has been estimated from the minimum of the temperature derivative of the magnetization, $dM = dT$, vs. temperature which has presented in the set of Figure 3.

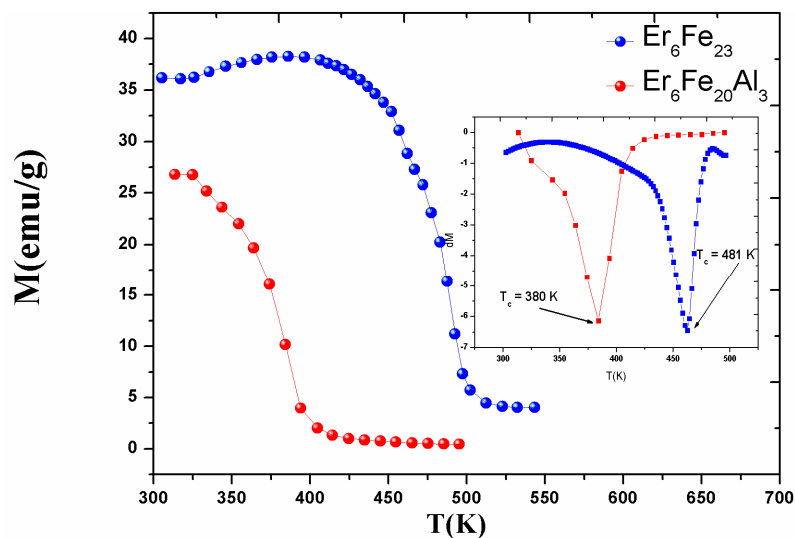


Figure 3. Temperature dependence of magnetization of $\text{Er}_6\text{Fe}_{23-x}\text{Al}_x$ with $x = 0$ and 3 under a low applied magnetic field $\mu_0H = 0.1$ T.

For $x = 0$, the T_C is equal to 481 K. The magnetic result is in good agreement with those already reported [10,25]. In the compound $\text{Er}_6\text{Fe}_{23}$, moments of erbium and iron couples antiparallel and the Curie temperature depends on the interactions Fe–Fe, Er–Fe and Er–Er [25]. The large exchange interaction depends on the Fe–Fe distance. It is obvious that the Fe–Fe interactions play the most significant role in the magnetic order of $\text{Er}_6\text{Fe}_{23}$ compound.

The magnetic transition T_C decreases from 481 K, for $x = 0$, to 380 K, for $x = 3$. We can conclude in the case of ternary $\text{Er}_6\text{Fe}_{20}\text{Al}_3$ that the interatomic-distance Fe–Fe decreases with increasing the content of aluminum. When Fe is substituted by non-magnetic Al, Fe–Fe interactions become weaker, leading to a Curie temperature decrease and a tendency magnetic disorder. According to the dilution law [26], when iron atoms are substituted by aluminum atoms, the magnetization of the sublattice decreases and, consequently, the molecular magnetic moment of the compound increases because the magnetization of the erbium sublattice in $\text{Er}_6\text{Fe}_{23}$ is larger than the iron sublattice. This decrease of Curie temperature is comparable with a system having a same type of structure ($\text{Th}_6\text{Mn}_{23}$), in the magnetic properties of $\text{Gd}_6(\text{Mn}_{1-x}\text{Fe}_x)_{23}$ alloys ($x < 0.2$) [27], the substitution of Mn by Fe leads to a decrease of the T_C down to 175 K for $x = 0.2$ [27–31].

Figure 4 shows that the $\text{Er}_6\text{Fe}_{20}\text{Al}_3$ compound has a minimum magnetization at 75 K. Indeed, the net moment at low temperature points in the direction of the Er moment, while in others, it points in the direction of the Fe moment, as evidenced by the presence of the compensation temperature at $T_{\text{comp}} = 75$ K. Before this temperature, the Er free ion moment coupled antiparallel to the Fe moments. The magnetic properties of the $\text{Er}_6\text{Fe}_{20}\text{Al}_3$ sample can readily be understood in reference to the $\text{Er}_6\text{Fe}_{23}$

compound from a model in which the Er moments are coupled antiparallel to the iron moments. This behavior is similar to the $\text{Er}_6\text{Fe}_{23}$ magnetic behavior ($T_{\text{comp}} = 95 \text{ K}$). This decrease is due to substitution by the Al atoms, and is comparable with the $\text{Er}_{6-x}\text{Y}_x\text{Fe}_{23}$ [32]. The magnetic saturations at 300 K of $\text{Er}_6\text{Fe}_{23-x}\text{Al}_x$ ($x = 0$ and 3) are about 14.74 and 10.24 μ_{B} , respectively.

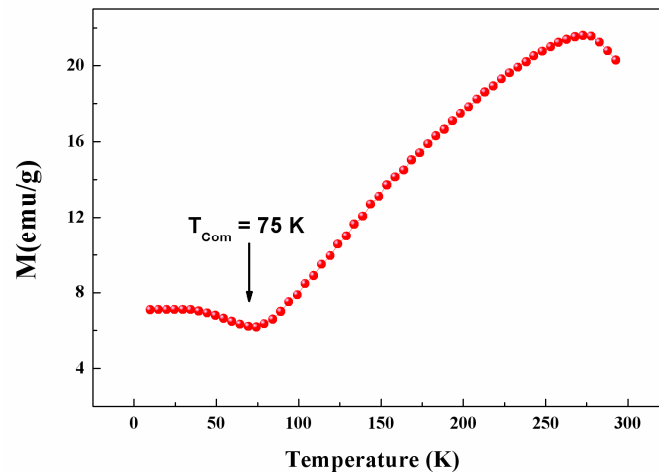


Figure 4. Shows temperature dependences of magnetization for $\text{Er}_6\text{Fe}_{20}\text{Al}_3$ compound under a magnetic field of 0.05 T.

3.3. Magnetocaloric Effect

In order to understand the influence of Al substitution in the magnetocaloric properties, we plotted the magnetization vs. the applied magnetic field (from 0 to 14 KOe) obtained at various temperatures for the $\text{Er}_6\text{Fe}_{23-x}\text{Al}_x$ ($x = 0$ and 3) samples in Figure 5. These curves provide evidence of a close relationship between the magnetization M and the applied magnetic field H . Below T_{C} , the magnetization M increases sharply with magnetic applied field for ($H < 0.5 \text{ kOe}$) and then saturates above 1 kOe. The saturation magnetization shifts to higher values with the decreasing temperature. When the temperature approaches T_{C} , the magnetization change becomes large.

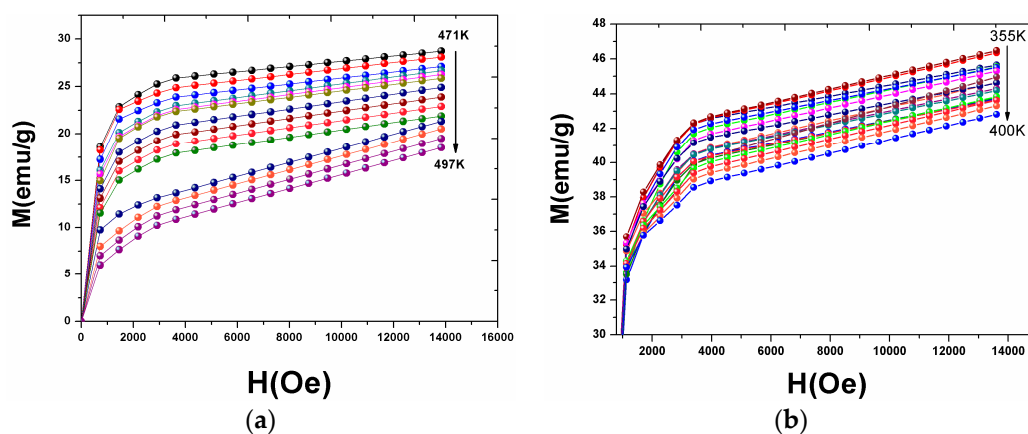


Figure 5. Magnetization versus applied magnetic field isotherms measured for $\text{Er}_6\text{Fe}_{20}\text{Al}_3$ (a) and $\text{Er}_6\text{Fe}_{23}$ (b) compounds.

To explain with precision the Curie temperature and the transition nature, the Arrott plots obtained from the magnetic field dependence of isothermal magnetization, are shown in Figure 6. The Banerjee criterion [33] has been used to determine the nature of the magnetic phase transition in

intermetallics. The positive or negative slope of M^2 vs $\mu_0 H/M$ (Arrott plot) curves indicates whether the magnetic phase transition is second or first order, respectively. In this compound, the positive slope of the Arrott plots confirms a characteristic of the second-order magnetic transition.

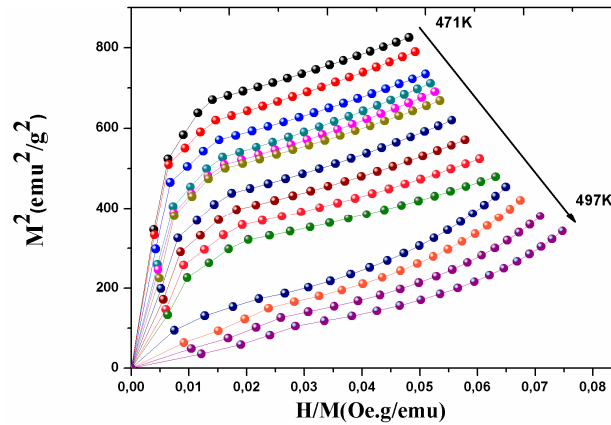


Figure 6. Arrott curves for $\text{Er}_6\text{Fe}_{23}$ intermetallic (as an example).

The magnetocaloric properties of $\text{Er}_6\text{Fe}_{23-x}\text{Al}_x$ have been calculated from magnetization vs. applied magnetic field ($M(H)$) curves, measured for temperatures within a 50 K interval centered around the T_C of each sample. The desired entropy variation $\Delta S(T)$ is then investigated, following the Maxwell relation [34,35] (Equation (1))

$$\Delta S_M(T, H) = S_M(T, H) - S_M(T, 0) = \int_0^{\mu_0 H_{\max}} \left(\frac{\partial S(T, H)}{\partial H} \right)_T dH \quad (1)$$

From Maxwell's thermodynamic relation (Equation (2))

$$\left(\frac{\partial S_M(T, H)}{\partial H} \right)_T = \left(\frac{\partial M(T, H)}{\partial T} \right)_H \quad (2)$$

One can obtain the following expression (Equation (3))

$$\Delta S_M(T, \Delta H)_{\Delta H} = \int_0^{\mu_0 H_{\max}} \left(\frac{\partial M(H, T)}{\partial T} \right)_H dH \quad (3)$$

where M is the magnetization, T is the temperature, and $\mu_0 H_{\max}$ is the maximum external field, with $\mu_0 = 1$ (c.g.s).

The Figure 7 presents the magnetic entropy change ΔS_M for both samples as a function of temperature under different magnetic fields. A remarkable feature is the exact correspondence between the maximal ΔS_M and the recorded ferrimagnetic transition at T_C , while ΔS_M distributes over a relatively wide T range. The maximum entropy change of only 0.58 J/kg K and 1.8 J/kg K upon a field variation of 14 kOe was obtained for $\text{Er}_6\text{Fe}_{20}\text{Al}_3$ and $\text{Er}_6\text{Fe}_{23}$, respectively, indicating relatively small magnetic order fluctuations around the ferrimagnetic transitions.

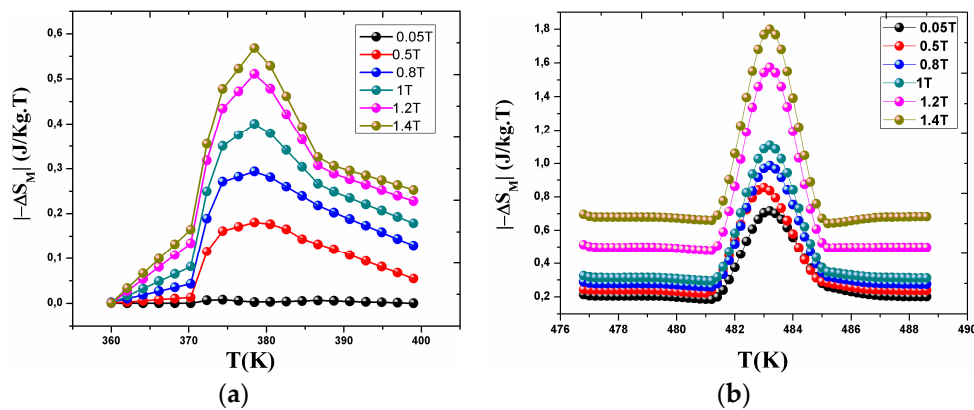


Figure 7. Isothermal magnetic entropy change around the Curie temperature for $\text{Er}_6\text{Fe}_{20}\text{Al}_3$ (a) and $\text{Er}_6\text{Fe}_{23}$ (b) compounds.

For the materials actually used in magnetic refrigeration, the most meaningful parameter is the relative cooling power (RCP). The RCP based on the magnetic entropy change ΔS_M is defined as [3,36,37]

$$\text{RCP} = |-\Delta S_M(T, H)| \times \delta T_{\text{FWHM}} \quad (4)$$

where δT_{FWHM} is the full-width at half the maximum of the magnetic entropy change curve. The calculated RCP values for $\Delta H = 14$ kOe are 28 and 42 J/kg K for $\text{Er}_6\text{Fe}_{20}\text{Al}_3$ and $\text{Er}_6\text{Fe}_{23}$, respectively. The RCP values show a difference between the two samples, due to the Fe/Al substitution.

We list in Table 3 the T_C , the ΔS_M (max), and the RCP values for our materials with 14 kOe magnetic applied field in comparison with other results reported in the literature. The lower values of (ΔS_M (max)) compared with those of the $\text{Er}_6\text{Fe}_{23-x}\text{Al}_x$ compounds are explained by the small value of the iron magnetic moment which is associated with a non-collinear Er magnetic structure. The magnetic entropy depends on the magnetic applied field and the nature of rare-earth.

Table 3. Curie temperature T_C , magnetic entropy change (ΔS_M), and relative cooling power (RCP) for R_6M_{23} compounds

Compound	T_C (K)	H (kOe)	ΔS_M (max) (J/kg·K)	RCP (J/kg)	Reference
Y_6Mn_{23}	505	50	2.1	-	[38]
$\text{Nd}_6\text{Mn}_{23}$	441	50	2.9	-	[38]
$\text{Sm}_6\text{Mn}_{23}$	456	50	2.6	-	[38]
$\text{Er}_6\text{Mn}_{23}$	430	50	34.3	-	[38]
$\text{Dy}_6\text{Mn}_{23}$	447	50	24.6	-	[38]
$\text{Gd}_6\text{Mn}_{23}$	489	10	1.6	-	[38]
$\text{Gd}_6(\text{Mn}_{0.875}\text{Co}_{0.125})_{23}$	265	10	2.4	-	[38]
$\text{Gd}_6(\text{Mn}_{0.85}\text{Co}_{0.15})_{23}$	219	10	2.9	-	[38]
$\text{Er}_6\text{Fe}_{20}\text{Al}_3$	481	14	0.58	28	This work
$\text{Er}_6\text{Fe}_{23}$	380	14	1.8	42	This work

4. Conclusions

In conclusion, we determined the effect of the Al substitution on the magnetic behavior, magnetic phase transition and magnetocaloric properties of $\text{Er}_6\text{Fe}_{23-x}\text{Al}_x$ ($x = 0$ and 3) compounds. The structural study revealed that the samples with $x = 0$ and 3 were crystallized in the cubic $\text{Th}_6\text{Mn}_{23}$ type structure. In addition, the Curie temperature decreased with increasing Al concentration. We have found that the samples under went a second-order magnetic phase transition. The decrease of T_C was accompanied by a reduction of the isothermal entropy change. For a magnetic field change of 0–14 kOe, a maximum magnetic entropy values of 0.58 J/kg·K and 1.8 J/kg·K for $\text{Er}_6\text{Fe}_{23-x}\text{Al}_x$

($x = 0$ and 3) compounds are determined around T_C . The values of this parameter are lower than those reported in $\text{Th}_6\text{Mn}_{23}$ alloys, which can be attributed to the presence of the contribution of Er free moment antiparallel to the Fe moment in this system.

Acknowledgments: This paper was written within the frame work of collaboration is supported by the Tunisian Ministry of Higher Education and Scientific Research and Technology and the Higher Education, Scientific of French (PHC MAGHREB project 15MAG07).

Author Contributions: Lotfi Bessais analyzed the data and wrote the paper, Mosbah Jemmali performed the experiments and analyzed the data, Essebti Dhahri and Safia Alleg provided with the samples.

Conflicts of Interest: The authors declare no conflict of interest.

References

1. Phejar, M.; Paul-Boncour, V.; Bessais, L. Structural and magnetic properties of magnetocaloric $\text{LaFe}_{13-x}\text{Si}_x$ compounds synthesized by high energy ball-milling. *Intermetallics* **2010**, *18*, 2301–2307. [[CrossRef](#)]
2. Nouri, K.; Jemmali, M.; Walha, S.; Zehani, K.; Ben Salah, A.; Bessais, L. Structural, atomic Hirschfeld surface, magnetic and magnetocaloric properties of SmNi_5 compound. *J. Alloys Compd.* **2016**, *672*, 440–448. [[CrossRef](#)]
3. Boutahar, A.; Lassri, H.; Zehani, K.; Bessais, L.; Hlil, E.K. Magnetic properties and magnetocaloric effect in amorphous $\text{Co}_{35}\text{Er}_{65}$ ribbon. *J. Magn. Magn. Mater.* **2014**, *369*, 92–95. [[CrossRef](#)]
4. Dhahri, A.; Jemmali, M.; Taibi, K.; Dhahri, E.; Hlil, E.K. Structural, magnetic and magnetocaloric properties of $\text{La}_{0.7}\text{Ca}_{0.2}\text{Sr}_{0.1}\text{Mn}_{1-x}\text{Cr}_x\text{O}_3$ compounds with $x = 0, 0.05$ and 0.1 . *J. Alloys Compd.* **2015**, *618*, 488–496. [[CrossRef](#)]
5. Bejar, M.; Dhahri, R.; El Halouani, F.; Dhahri, E. Magnetocaloric effect at room temperature in powder of $\text{La}_{0.5}(\text{CaSr})_{0.5}\text{MnO}_3$. *J. Alloys Compd.* **2006**, *414*, 31–35. [[CrossRef](#)]
6. Triki, M.; Dhahri, R.; Bekri, M.; Dhahri, E.; Valente, M.A. Magnetocaloric effect in composite structures based on ferromagnetic–ferroelectric $\text{Pr}_{0.6}\text{Sr}_{0.4}\text{MnO}_3/\text{BaTiO}_3$ perovskites. *J. Alloys Compd.* **2011**, *509*, 9460–9465. [[CrossRef](#)]
7. Barclay, J.; Oseen-Senda, K.; Skrzypkowski, M. Unique feature of liquefaction of hydrogen and natural. In Proceedings of the 6th IIF-IIR International Conference on Magnetic Refrigeration, Victoria, BC, Canada, 7–10 September 2014.
8. Numazawa, T.; Kamiya, K.; Utaki, T.; Matsumoto, K. Magnetic refrigerator for hydrogen liquefaction. *Cryogenics* **2014**, *62*, 185–192. [[CrossRef](#)]
9. Pecharsky, V.K.; Gschneidner, K.A., Jr.; Mudryk, Y.; Paudyal, D. Making the most of the magnetic and lattice entropy changes. *J. Magn. Magn. Mater.* **2009**, *321*, 3541–3547. [[CrossRef](#)]
10. Boltich, E.B.; Pourarian, F.; Wallace, W.E.; Smith, H.K.; Malik, S.K. Influence of hydrogen on structure and magnetic properties of $\text{Ho}_6\text{Fe}_{23}$ and $\text{Er}_6\text{Fe}_{23}$. *Solid State Commun.* **1981**, *40*, 117–120. [[CrossRef](#)]
11. Pedziwiatr, A.T.; Smith, H.K.; Wallace, W.E. Magnetic and structural characteristics of $\text{Ho}_6\text{Fe}_{23}$ deuterides. *J. Solid State Chem.* **1983**, *47*, 41–46. [[CrossRef](#)]
12. Laguna-Marco, M.A.; Chaboy, J.; Maruyama, H. Temperature dependence of the Ho $L_{2,3}$ -edges XMCD spectra in $\text{Ho}_6\text{Fe}_{23}$. *Physica B* **2004**, *345*, 197–200. [[CrossRef](#)]
13. Ouladdiaf, B.; Deportes, J.; Rodriguez-Carvajal, J. Magnetic structures of $\text{Er}_6\text{Mn}_{23}$ and $\text{Dy}_6\text{Mn}_{23}$. *Physica B* **1995**, *213*, 330–332. [[CrossRef](#)]
14. Delapalme, A.; Deportes, J.; Lemaire, R.; Hardman, K.; James, W.J. Magnetic interactions in R_6Mn_{23} rare earth intermetallics. *J. Appl. Phys.* **1979**, *50*, 1987. [[CrossRef](#)]
15. Hardman, K.; James, W.J.; Deportes, J.; Lemaire, R.; de la Bathie, R.P. Magnetic properties of R_6Mn_{23} compounds. *J. Phys. Colloq.* **1979**, *40*, C5–C204. [[CrossRef](#)]
16. Buschow, K.H.J.; Sherwood, R.C. Magnetic properties and hydrogen absorption in rare-earth intermetallics of the type RMn_2 and R_6Mn_{23} . *J. Appl. Phys.* **1977**, *48*, 4643. [[CrossRef](#)]
17. Buschow, K.H.J. Magnetic properties of the ternary hydrides of $\text{Nd}_6\text{Mn}_{23}$ and $\text{Sm}_6\text{Mn}_{23}$. *Solid State Commun.* **1981**, *40*, 207. [[CrossRef](#)]
18. Parker, F.T.; Oesterreicher, H. Analysis of magnetic interactions and structure in R_6Mn_{23} . *Appl. Phys. A* **1982**, *27*, 65. [[CrossRef](#)]

19. Buschow, K.H.J.; Gubbens, P.C.M.; Ras, W.; van der Kraan, A.M. Magnetization and Mössbauer effect study of Dy₆Mn₂₃ and Tm₆Mn₂₃ and their ternary hydrides. *J. Appl. Phys.* **1982**, *53*, 8329. [[CrossRef](#)]
20. Rietveld, H. A profile refinement method for nuclear and magnetic structures. *J. Appl. Crystallogr.* **1969**, *2*, 65. [[CrossRef](#)]
21. Jemmali, M.; Walha, S.; Pasturel, M.; Tougait, O.; Hassen, R.B.; Noël, H. Isothermal section of the Er–Fe–Al ternary system at 800 °C. *J. Alloys Compd.* **2010**, *21*, 421–423. [[CrossRef](#)]
22. Kropyakevych, P.I.; Frankevich, D.P.; Voroshilov, Y.V. Compounds with Th₆Mn₂₃-type structures in alloys of the rare-earth metals with manganese and iron. *Sov. Powder Metall. Met. Ceram.* **1965**, *4*, 915–919. [[CrossRef](#)]
23. Jemmali, M.; Walha, S.; Ben Hassen, R.; Noël, H. Synthesis and Crystal Structure of Er₆Fe_{17.66}Al_{15.34}Co_{0.65} Intermetallic Compound. *Jpn. Soc. Anal. Chem.* **2009**, *25*, 123–124. [[CrossRef](#)]
24. Lemoine, P.; Verniere, A.; Malaman, B.; Mazet, T. Magnetic and magnetocaloric properties of Gd₆(Mn_{1-x}Co_x)₂₃ compounds (x ≤ 0.3). *J. Alloys Compd.* **2016**, *680*, 612–616. [[CrossRef](#)]
25. Herbst, J.F.; Croat, J.J.; Van Laar, B.; Yelon, W.B. Magnetic structure of Er₆Fe₂₃. *J. Appl. Phys.* **1984**, *56*, 1224–1226. [[CrossRef](#)]
26. Walha, S.; Jemmali, M.; Skini, R.; Noel, H.; Dhahri, E.; Hassen, R.B.; Hlil, E.K. Structural and Magnetocaloric Properties of ErFe_{2.4}Al_{0.6} Compound. *J. Supercond. Nov. Magn.* **2014**, *27*, 2131–2137. [[CrossRef](#)]
27. Lemoine, P.; Ban, V.; Verniere, A.; Mazet, T.; Malaman, B. Magnetocaloric properties of View the MathML source alloys (x ≤ 0.2). *Solid State Commun.* **2010**, *150*, 1556. [[CrossRef](#)]
28. Kirchmayr, H.R.; Steiner, W. Magnetic order of the compound series RE₆(Mn_xFe_{1-x})₂₃ (RE = Y, Gd). *J. Phys. Colloq.* **1971**, *32*, 665–667. [[CrossRef](#)]
29. Wallace, W.E. *Rare Earth Intermetallics*; Academic Press: Cambridge, MA, USA, 1973; ISBN 9780127328508.
30. Nagai, H.; Oyama, N.; Ikami, Y.; Yoshie, H.; Tsujimura, A. The Magnetic Properties of Pseudo-Binary Compounds, Gd(Fe_{1-x}Mn_x)₂ and Gd₆(Fe_{1-y}Mn_y)₂₃. *J. Phys. Soc. Jpn.* **1986**, *55*, 177. [[CrossRef](#)]
31. Nagai, H.; Yokoyama, T.; Katsuyama, S.; Amako, Y.; Yoshie, H.; Adachi, K. The anomalous behaviour of the electrical resistivities of Gd(Fe,Mn)₂ and Gd₆(Fe,Mn)₂₃. *J. Magn. Magn. Mater.* **1998**, *1131–132*, 177–181. [[CrossRef](#)]
32. Pedziwiatr, A.T.; Boltich, E.B.; Wallace, W.E.; Craig, R.S. Magnetic and structural properties of Y_{6-x}Er_xFe₂₃ alloys and their hydrides. *J. Solid State Chem.* **1983**, *46*, 342–348. [[CrossRef](#)]
33. Banerjee, S.K. On a generalised approach to first and second order magnetic transitions. *Phys. Lett.* **1964**, *12*, 16. [[CrossRef](#)]
34. Yu, B.F.; Gao, Q.; Zhang, B.; Meng, X.Z. Review on research of room temperature magnetic refrigeration. *Chin. Int. J. Refrig.* **2003**, *26*, 622–636. [[CrossRef](#)]
35. Pecharsky, V.K., Jr.; Gschneidner, K. Magnetocaloric effect from indirect measurements: Magnetization and heat capacity. *J. Appl. Phys.* **1999**, *86*, 565. [[CrossRef](#)]
36. Gschneider, K.A.; Pecharsky, V.K.; Tsokol, A.O. Recent developments in magnetocaloric materials. *Rep. Prog. Phys.* **2005**, *68*, 1479. [[CrossRef](#)]
37. Boutahar, A.; Lassri, H.; Hlil, E.K.; Suprercond, J. Low Temperature Giant Magnetocaloric Effect and Critical Behavior in Amorphous Co_{100-x}Er_x (x = 55, 65) Alloys. *Nov. Magn.* **2014**, *27*, 2865. [[CrossRef](#)]
38. Lemoine, P.; Verniere, A.; Mazet, T.; Magn, B.M. Magnetic and magnetocaloric properties of R₆Mn₂₃ (R=Y, Nd, Sm, Gd-Tm, Lu) compounds. *J. Magn. Magn. Mater.* **2011**, *323*, 2690–2695. [[CrossRef](#)]

